Graphene-passivated nickel as an efficient hole-injecting electrode for large area organic semiconductor devices

Daniele Di Nuzzo[1]*, Ryo Mizuta[2], Kenichi Nakanishi[2], Marie-Blandine Martin[3], Adrianus I. Aria[4], Robert Weatherup[5], Richard H. Friend[1], Stephan Hofmann[2], Jack Alexander-Webber[2]*

[1] Cavendish Laboratory, University of Cambridge, Cambridge, CB3 0HE, United Kingdom

[2] Department of Engineering, University of Cambridge, Cambridge CB3 0FA, United Kingdom

[3] Thales Research and Technology, 1 avenue Augustin Fresnel, 91767 Palaiseau, France

[4] Surface Engineering and Precision Institute, School of Aerospace, Transport and Manufacturing, Cranfield University, Cranfield, MK43 0AL, United Kingdom

[5] Department of Materials, University of Oxford, Parks Road, Oxford, OX1 3PH, United Kingdom

Email: dd467@alumni.cam.ac.uk (D.D.N)
Email: jaa59@cam.ac.uk (J.A.-W.)

ABSTRACT

Efficient injection of charge from metal electrodes into semiconductors is of paramount importance to obtain high performance optoelectronic devices. The quality of the interface between the electrode and the semiconductor must therefore be carefully controlled. The case of organic semiconductors presents specific problems: ambient deposition techniques, such as solution processing, restrict the choice of electrodes to those not prone to oxidation, limiting potential application. Additionally, damage to the semiconductor in sputter coating or high temperature thermal evaporation poses an obstacle to the use of many device-relevant metals as top electrodes in vertical metal-semiconductor-metal structures, making it preferable to use them as bottom electrodes. Here we propose a possible solution to these problems by implementing graphene-passivated nickel as an air stable bottom electrode in vertical devices comprising organic semiconductors. We use these passivated layers as hole-injecting bottom electrodes and we show that efficient charge injection can be achieved into standard organic semiconducting polymers, owing to an oxide free nickel/graphene/polymer

1

interface. Crucially, we fabricate our electrodes with low roughness, which in turn allows us to produce large area devices (of the order of millimetre squares) without electrical shorts occurring. Our results make these graphene-passivated ferromagnetic electrodes a promising approach for large area organic optoelectronic and spintronic devices.

Organic semiconductors serve as a platform for (opto)electronic devices with tuneable characteristics by molecular design, enabling versatile device integration and processing strategies.[1] However, ambient processing techniques such as solution processing can facilitate oxidation of metal contacts, resulting in an uncontrolled electronic interface which is deleterious to performance in semiconductor devices.[2,3] New techniques are therefore required to control the interface between organic semiconductors and oxidising metals while maintaining the possibility of solution processing.

Graphene has been shown to act as an atomically thin permeation barrier.[4–6] Graphene grown via chemical vapour deposition (CVD) directly on the surface of strongly interacting[7] catalytic metals, such as Ni, Co or Fe, acts as a barrier layer to prevent oxidation.[8–11] These oxide-free ferromagnetic interfaces have been shown to hold significant benefits within the field of spintronics,[12,13] as they enable oxidative fabrication processes, such as solution processing[9,10] or atomic layer deposition,[14] to be used to fabricate devices with a wider range of relevant materials. One appealing possibility would be to develop graphene-passivated ferromagnets as electrodes[9,10] for organic semiconductor spintronics,[15–18] where the quality of the electronic interface between ferromagnetic electrode and organic semiconductor is of paramount importance.[19,20] Another important advantage of an ambient-stable ferromagnetic layer is that it can be used as a bottom electrode in vertical metal-organic semiconductor-metal structures, allowing to employ techniques such as sputtering to obtain high quality and thickness-controlled metal layers or multi-layers; note that sputtering cannot be used for top-electrodes as it would destroy[21] the organic semiconductor.

Previous reports using graphene passivated ferromagnets as electrodes for organic semiconductor devices have studied the spin injection properties[10] as well as charge injection in lateral organic semiconductor field effect transistors[9]. In this work we investigate few-layer graphene-passivated nickel (Ni/FLG) as a bottom electrode for injection of holes into organic semiconducting polymers, demonstrating efficient injection into two standard semiconducting polymers deposited from solution, and in air, directly on top of Ni/FLG.

Compared to previous reports on graphene-passivated ferromagnetic electrodes, where lithographic techniques had to be used in order to produce micrometre-sized features,[8–10,14,22] here we were able to produce working devices with orders of magnitude larger active area (4.5 mm^2). Our results are thus encouraging for the further development of organic optoelectronic and spintronic devices processed from solution under ambient conditions.
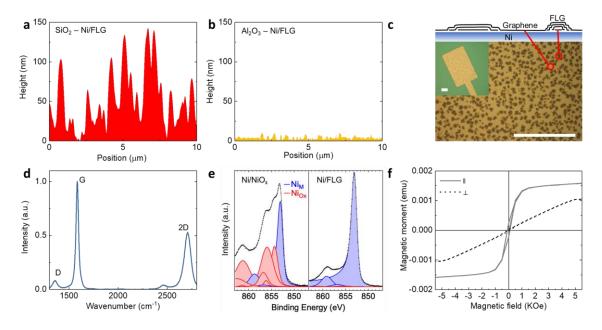
Nickel was initially sputtered on thermally oxidised silicon wafers, producing films with a thickness of 150 nm. FLG domains were grown on such sputtered Ni films in a custom low-pressure Chemical Vapour Deposition (CVD) reactor (base pressure ~1E-6 mbar). All substrates were cleaned by sonicating in acetone followed by isopropyl alcohol, and blow-dried with a nitrogen gun before loading. Samples were heated to approximately 450 °C using a resistive heater (temperature measurements by a K-type thermocouple) with a rapid ramp rate of 100 °C/min, and annealed in ~1 mbar of H$_2$ for 10 minutes. This acts to reduce the native oxide prior to graphene growth. After annealing, the H$_2$ flow was stopped and the chamber was evacuated back to approximately base pressure over a period of 5 minutes. For graphene growth, C$_2$H$_2$ gas was gradually introduced into the reactor via a mass flow controller by incrementally increasing the flow rate over 5 minutes to achieve a partial pressure of C$_2$H$_2$ of 2.5E-4 mbar. Subsequently, the samples were held at 450 °C in 2.5E-4 mbar of C$_2$H$_2$ for a further 25 minutes, before rapidly cooling (initially ~300 °C/min) whilst maintaining the C$_2$H$_2$ flow. All gases were stopped once room temperature had been reached.

Upon graphene growth, a roughening of the Ni sputtered on thermally oxidised Si was observed, with an RMS = 67 nm (**Fig. 1a**). The roughness was found to increase with increasing growth temperature. The roughening of Ni upon graphene growth is explained by grain growth in the sputtered Ni films, occurring at the high temperatures during the CVD process: under these conditions, the internal forces in the film are larger than those between the film and the substrate, and diffusion of the film material is appreciable.

Surface roughness is a significant problem in our desired vertical metal-semiconductor-metal devices: to obtain the cleanest interface and achieve efficient charge injection, the organic semiconductors are spin coated from solution directly on top of the Ni–graphene film without the use of roughness-reducing intermediate layers; however, if the surface of the Ni–graphene film is too rough, Ni protrudes through the film and can directly contact the top electrode, causing electrical shorting of the devices. While a thick layer of organic semiconductor may be used to contain this problem, the operating voltage of the devices will scale with the

3

semiconductor thickness, resulting in impractical voltages being required to operate the devices.

To solve the issue of roughness, we reduced grain growth by adding a 10 nm Al_2O_3 adhesion-promoting layer,[23] grown by atomic layer deposition on the Si wafer prior to Ni deposition. The Al_2O_3 adhesion-promoting layer sensibly reduced the surface roughness (**Fig. 1b**, RMS = 4.3nm): as presented below, this allowed us to reliably fabricate working devices showing no electrical shorts and with a surface area of 4.5 mm^2, which is large compared to commonly studied vertical spintronic devices (typically on a scale between 1 and 10^4 micrometre-square).[8–10,14,22]

Fig. 1. *AFM line scan of sputtered Ni films after graphene growth using a Si–SiO₂ substrate without (a) and with (b) an Al₂O₃ adhesion layer. (c) Optical micrograph of a graphene-passivated Ni electrode, including a cartoon indicating areas with different numbers of graphene layers. Scale bars are 50μm. (d) Raman spectrum of few-layer graphene on Ni. (e) XPS of Ni 2p₃/₂ region of sputtered Ni (Ni/NiOₓ – black) and Ni after multilayer graphene growth (Ni/FLG – green), with peak fitting indicating metallic nickel (NiₘM) and nickel oxide (NiₒOx). (f) Magnetic moment measured at room temperature by DC-mode SQUID magnetometry of graphene-passivated Ni films for magnetic fields parallel (grey, solid) and perpendicular (black, dots) to the plane of the film.*

Optical microscopy (**Fig. 1c**) and Raman spectroscopy (**Fig. 1d**) confirmed that the electrodes were fully covered with graphene, notably with islands of multiple layers, as is often observed under similar growth conditions on Ni thin films.[11,24,25] Such thicker multilayer islands appeared as dark sections in optical microscopy, as shown schematically in **Fig. 1c**.

Raman spectroscopy was carried out using a Renishaw inVia confocal Raman microscope, and a laser excitation wavelength of 532nm. We observed a D peak (**Fig. 1d**), which we ascribe to the relatively low temperature of the growth process. The broad 2D peak (FWHM = 79 cm^{-1}) and G/2D ratio >1 is also consistent with multilayer growth.[26]

X-ray photoelectron spectroscopy (XPS) was measured using a Thermo Scientific ESCALAB 250Xi with a micro-focussed and monochromated Al Kα X-ray source. All spectra were background- corrected (Shirley) and analysed by performing a nonlinear mean square fit of the data, using Doniach-Šùnjić functions convoluted with Gaussian profiles. Measurements of the $Ni2p_{3/2}$ region confirmed that the sputtered Ni is initially oxidised during air transfer, with significant nickel oxide/hydroxide (Ni_{Ox}) components visible (**Fig. 1e left**). Following graphene growth, the previously oxidised Ni is reduced to metallic Ni, and remains reduced despite transfer of the electrodes through air, as confirmed by the dominant Ni_M components and negligible contributions from Ni_{Ox} species (**Fig. 1e right**). This effective passivation is attributable to the strong interaction between graphene and Ni, and the fact that even if defects are present in the graphene, a passivating oxide is formed locally which does not propagate laterally.[27] Herein, we used an extended hydrocarbon exposure with the intention of blocking as many defects as possible through the formation of thicker FLG at these locations, where hydrocarbon can continue to access the Ni surface (**Fig. 1c**).

We used a Quantum Design SQUID magnetometer (MPMS3 model) to determine the room temperature magnetic properties of the Ni films after graphene growth (**Fig. 1f**). With a standard DC-mode measurement we determined the magnetization of our films parallel and perpendicular to the magnetic field: consistent with previous observations,[28] the easy-axis of magnetization of the Ni films is parallel to the plane of the film. The films also show the typical small hysteresis of nickel being a "soft" ferromagnetic metal. These measurements thus confirm that the bulk ferromagnetic properties of the Ni layers are maintained after graphene passivation.
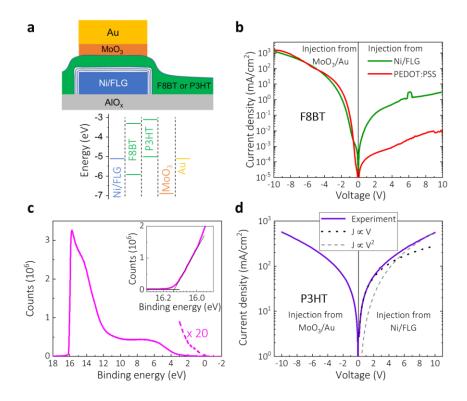
We then fabricated devices with the structure schematically depicted in **Fig. 2a**. Electrodes consisting of 150 nm thick stripes of Ni were patterned by using shadow masks on a Si wafer with an Al_2O_3 adhesion layer; few-layer graphene was grown on top of Ni as described above. We first studied hole injection into the organic semiconducting polymer F8BT (poly(9,9-dioctylfluorene-alt-benzothiadiazole), a polymer commonly used in green emitting OLEDs. F8BT was previously received from Cambridge Display Technology and it was spin coated in air directly on top of the bottom electrode. A solution of 15 mg/mL in para-xylene

was used for spin-coating, giving smooth and homogeneous films with a thickness of 180 nm (measured with a Dektak profilometer). A top electrode consisting of MoO_3/Au (8 nm/100 nm) was then deposited by thermal evaporation at a pressure of 10^{-7} mbar.

The device area, determined by the overlap of the top and bottom contacts, was 4.5 mm^2. The MoO_3/Au contact was used to study ohmic injection into the deep-lying HOMO level of F8BT (-5.9 eV).[29] Ohmic injection of holes has been demonstrated previously using MoO_3 and is due to surface p-doping of the polymer by the MoO_3 at the polymer interface[30] which results in barrier-free injection.[31] **Fig. 2b** shows the *current density – voltage* characteristic measured on the devices. Negative voltages correspond to injection of holes from MoO_3/Au: ohmic injection is achieved as expected, evidenced by high currents reaching the space-charge limit at high absolute voltages.

The Ni/FLG devices were compared against reference devices having the same surface area and consisting of the standard structure ITO/PEDOT:PSS/F8BT/MoO_3/Au. For PEDOT:PSS, the Heraeus Clevios™ AI 4083 formulation was used. The PEDOT:PSS film was deposited in air on top of a cleaned, pre-patterned ITO substrate and subsequently annealed under nitrogen for 20 minutes at 150 °C. The remaining part of the vertical stack was fabricated as in the case of Ni/FLG-based devices.

When injecting from MoO_3/Au, the same behaviour as in the Ni/FLG devices was observed. When injecting from PEDOT:PSS into F8BT, current densities ca. five orders of magnitude lower were observed, consistent with injection of holes being barrier-limited. While we still observed a barrier-limited injection, when injecting holes from Ni/FLG we recorded current densities that were 2-3 orders of magnitude higher than in the case of PEDOT:PSS.

Fig. 2. *(a) Schematic representation of the device structure used. (b) Comparison of hole injection into F8BT from graphene-passivated Ni (green) and PEDOT:PSS (red) bottom contacts, each using a top contact of MoO₃ / Au. (c) Binding energy, referenced to the Fermi level, measured on a Ni/FLG sample by means of UPS (excitation light with energy hν = 21.21 eV). The inset shows the high binding energy part of the spectrum used to extract the cut-off energy E_{CO}. The work function ϕ is calculated as $\phi = h\nu - E_{CO}$. For better visualization, the part of the curve at the Fermi level is also shown after 20-fold magnification (dashed line). (d) Hole injection into P3HT from graphene-passivated Ni, with MoO₃ /Au top contact.*

We further characterized the Ni/FLG layers to obtain more information about their electrical properties in devices. We measured the resistivity of the Ni/FLG films using the four-point probe method and recorded a resistivity of 1.5E-7 Ω·m. This translates in a series resistance of the whole Ni/FLG lead of ~1 Ω, therefore representing a negligible contribution to the total resistance of the device.

We then measured the work function of our Ni/FLG substrates by means of ultraviolet photoelectron spectroscopy (UPS) in a Thermo Fisher Scientific ESCALAB 250Xi X-ray/Ultraviolet (XPS/UPS) photoelectron spectrometer, using an excitation wavelength of 21.21 eV: consistently with previous reports, our Ni/FLG samples show a work function of 5.07 eV (**Fig. 2c**), which is close to the work function of nickel.[32–34] A substantial energy
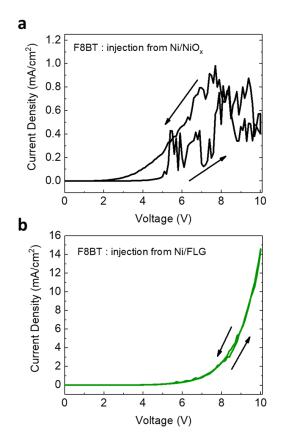
barrier is therefore present at the Ni/FLG/F8BT interface, resulting in the barrier-limited injection observed in **Fig. 2b**. Note that the measured work function of Ni/FLG is comparable to the work function of the same PEDOT:PSS formulation, previously reported as 5.1eV.[35] However, charge accumulation at the Ni/FLG/F8BT interface under voltage bias could shift the work function downwards, as it has been previously shown in graphene:[36,37] we hypothesise that this effect might contribute to a lower effective injection barrier at the interface with Ni/FLG compared to PEDOT:PSS, thus explaining the difference in current density observed at positive bias in F8BT-based devices (**Fig. 2b**).

We tested the same Ni/FLG/polymer/MoO$_3$/Au structure using another standard semiconducting polymer: P3HT (Poly(3-hexylthiophene-2,5-diyl)). P3HT was purchased from Rieke Metals in its regio-regular version (catalogue number RMI-00EE) and dissolved in a chlorobenzene:chloroform mixture (50:50, volume:volume) using a concentration of 30 mg/mL; spin-coating in air yielded smooth and homogeneous films of 200 nm thickness (measured with a Dektak profilometer). A MoO$_3$/Au (8/100nm) top electrode was evaporated on top of the polymer layer, as in the case of the previously discussed F8BT devices.

In this case we observed high currents both when injecting from MoO$_3$/Au and when injecting from Ni/FLG (**Fig. 2d**), with a very symmetric *current density – voltage* curve, linear at low voltages and reaching space-charge current limit at higher voltages (as testified by a V^2 dependence of the current density). The perfectly symmetric J-V plot demonstrates that hole injection in P3HT is barrier-free from both contacts. This result is consistent with the absence of an energy barrier between the HOMO level of P3HT (5.0 eV), and Ni/FLG (5.07 eV as measured in UPS).

To further investigate the electronic quality of nickel passivated electrodes, we compared the hole injection into F8BT from passivated nickel to the case of non-protected nickel electrodes (**Fig. 3**). Here we tested smaller scale devices with an active area of 0.05mm^2, fabricated by employing a resist mask patterned by photolithography for the deposition of Ni followed by lift-off in acetone. The applied voltage was set up to probe hole injection from the Ni/NiO$_x$ into F8BT. We observed that hole injection from unpassivated Ni/NiO$_x$ has a very low efficiency (**Fig. 3a**), indicated by low and unstable current densities. A significant improvement is observed with graphene passivation (**Fig. 3b**), suggesting that the native oxide of Ni has a detrimental effect on charge injection.

Furthermore, in **Fig. 3** the voltage is swept first from 0V to 10V and then 10V to 0V at a sweep rate of 2Vs^{-1} so that any hysteretic effects can be studied. Our Ni/NiO$_x$ devices show not only strong instabilities in current, but also large hysteretic behaviour. We explain the observed unstable and hysteretic currents as originating from resistive switching processes taking place in NiO$_x$. Resistive switching is well known to occur in NiO$_x$, supported by the presence of defects (e.g. oxygen vacancies).[38] The behaviour displayed by our Ni/NiO$_x$/F8BT devices suggests that conductive filaments of metallic nickel are formed in the NiO$_x$ native layer upon the application of the voltage bias, causing the spikes in current. A fraction of these conductive filaments is likely to persist during the whole sweep and to give rise to the hysteresis; note that the NiO$_x$ layer formed on our electrodes during air exposure is expected to be thin (a few nanometres),[39] resulting in large electric fields across it at the voltages used in this study. Supporting this interpretation, graphene-passivated electrodes do not show any significant hysteresis, while presenting a much higher density of injected current (**Fig. 3b**), consistent with the current densities in the large area device (**Fig. 2b**).

Fig. 3. Current density hysteresis as a function of voltage for hole injection into F8BT using (a) unprotected sputtered Ni electrodes and (b)graphene-passivated Ni. The arrows indicate the direction of voltage sweep.

In this work we were able to fabricate clean interfaces based on nickel passivated with few-layer graphene, providing efficient charge injection into solution-processed organic semiconductor layers. Crucially, we were able to fabricate such layers as bottom electrodes with very low roughness, which enabled their employment in large area vertical metal-semiconductor-metal devices, up to 2 orders of magnitude larger than previously reported organic devices, based on graphene-passivated cobalt.[10] Our results provide a route to retain two main advantages offered by organic semiconductors, large area and solution processing in air, while also producing high quality ferromagnetic electrodes with clean interfaces, a necessary requisite for achieving high performance optoelectronic and, particularly, spintronic devices.

REFERENCES

[1] C. Wang, H. Dong, W. Hu, Y. Liu, and D. Zhu, Chem. Rev. **112**, 2208 (2012).

[2] F. So and D. Kondakov, Adv. Mater. **22**, 3762 (2010).

[3] E. Voroshazi, B. Verreet, A. Buri, R. Müller, D. Di Nuzzo, and P. Heremans, Org. Electron. Physics, Mater. Appl. **12**, 736 (2011).

[4] J.S. Bunch, S.S. Verbridge, J.S. Alden, A.M. Van Der Zande, J.M. Parpia, H.G. Craighead, and P.L. McEuen, Nano Lett. **8**, 2458 (2008).

[5] V. Berry, Carbon **62**, 1 (2013).

[6] A.A. Sagade, A.I. Aria, S. Edge, P. Melgari, B. Gieseking, B.C. Bayer, J.C. Meyer, D. Bird, P. Brewer, and S. Hofmann, Npj 2D Mater. Appl. **1**, 35 (2017).

[7] Y.S. Dedkov and M. Fonin, New J. Phys. **12**, 125004 (2010).

[8] M.B. Martin, B. Dlubak, R.S. Weatherup, M. Piquemal-Banci, H. Yang, R. Blume, R. Schloegl, S. Collin, F. Petroff, S. Hofmann, J. Robertson, A. Anane, A. Fert, and P. Seneor, Appl. Phys. Lett. **107**, 012408 (2015).

[9] T. Verduci, C.S. Yang, L. Bernard, G. Lee, S. Boukari, E. Orgiu, P. Samorì, J.O. Lee, and B. Doudin, Adv. Mater. Interfaces **3**, 1500501 (2016).

[10] G. Zhou, G. Tang, T. Li, G. Pan, Z. Deng, and F. Zhang, J. Phys. D. Appl. Phys. **50**, 095001 (2017).

[11] A. Dahal and M. Batzill, Nanoscale **6**, 2548 (2014).

[12] M. Piquemal-Banci, R. Galceran, M.B. Martin, F. Godel, A. Anane, F. Petroff, B. Dlubak, and P. Seneor, J. Phys. D. Appl. Phys. **50**, 203002 (2017).

[13] P.U. Asshoff, J.L. Sambricio, A.P. Rooney, S. Slizovskiy, A. Mishchenko, A.M. Rakowski, E.W. Hill, A.K. Geim, S.J. Haigh, V.I. Fal'Ko, I.J. Vera-Marun, and I. V. Grigorieva, 2D Mater. **4**, 031004 (2017).

[14] M.B. Martin, B. Dlubak, R.S. Weatherup, H. Yang, C. Deranlot, K. Bouzehouane, F. Petroff, A. Anane, S. Hofmann, J. Robertson, A. Fert, and P. Seneor, ACS Nano **8**, 7890 (2014).

[15] J. Devkota, R. Geng, R.C. Subedi, and T.D. Nguyen, Adv. Funct. Mater. **26**, 3881 (2016).

[16] J.P. Prieto-Ruiz, S.G. Miralles, H. Prima-García, A. López-Muñoz, A. Riminucci, P. Graziosi, M. Aeschlimann, M. Cinchetti, V.A. Dediu, and E. Coronado, Adv. Mater. **31**, 1806817 (2019).

[17] X. Sun, S. Vélez, A. Atxabal, A. Bedoya-Pinto, S. Parui, X. Zhu, R. Llopis, F. Casanova, and L.E. Hueso, Science **357**, 677 (2017).

[18] D. Sun, E. Ehrenfreund, and Z.V. Vardeny, Chem. Commun. **50**, 1781 (2014).

[19] S. Zanettini, G. Chaumy, P. Chávez, N. Leclerc, C. Etrillard, B. Leconte, F. Chevrier, J.F. Dayen, and B. Doudin, J. Phys. Condens. Matter **27**, 462001 (2015).

[20] H. Ma, H.L. Yip, F. Huang, and A.K.Y. Jen, Adv. Funct. Mater. **20**, 1371 (2010).

[21] L.S. Liao, L.S. Hung, W.C. Chan, X.M. Ding, T.K. Sham, I. Bello, C.S. Lee, and S.T. Lee, Appl. Phys. Lett. **75**, 1619 (1999).

[22] M. Piquemal-Banci, R. Galceran, M.B. Martin, F. Godel, A. Anane, F. Petroff, B. Dlubak,

and P. Seneor, J. Phys. D. Appl. Phys. **50**, 203002 (2017).

[23] E. Ozceri and Y. Selamet, J. Phys. D. Appl. Phys. **48**, 455302 (2015).

[24] R.S. Weatherup, B. Dlubak, and S. Hofmann, ACS Nano **6**, 9996 (2012).

[25] A. Cabrero-Vilatela, R.S. Weatherup, P. Braeuninger-Weimer, S. Caneva, and S. Hofmann, Nanoscale **8**, 2149 (2016).

[26] A.C. Ferrari and D.M. Basko, Nat. Nanotechnol. **8**, 235 (2013).

[27] R.S. Weatherup, L. D'Arsié, A. Cabrero-Vilatela, S. Caneva, R. Blume, J. Robertson, R. Schloegl, and S. Hofmann, J. Am. Chem. Soc. **137**, 14358 (2015).

[28] B.L. Zink, M. Manno, L. O'Brien, J. Lotze, M. Weiler, D. Bassett, S.J. Mason, S.T.B. Goennenwein, M. Johnson, and C. Leighton, Phys. Rev. B **93**, 184401 (2016).

[29] Y. Zhang and P.W.M. Blom, Appl. Phys. Lett. **98**, 143504 (2011).

[30] M.C. Gwinner, R. Di Pietro, Y. Vaynzof, K.J. Greenberg, P.K.H. Ho, R.H. Friend, and H. Sirringhaus, Adv. Funct. Mater. **21**, 1432 (2011).

[31] D. Kabra, L.P. Lu, M.H. Song, H.J. Snaith, and R.H. Friend, Adv. Mater. **22**, 3194 (2010).

[32] H. Hibino, H. Kageshima, M. Kotsugi, F. Maeda, F.Z. Guo, and Y. Watanabe, Phys. Rev. B **79**, 125437 (2009).

[33] S.M. Song, J.K. Park, O.J. Sul, and B.J. Cho, Nano Lett. **12**, 3887 (2012).

[34] S.M. Song, J.H. Bong, and B.J. Cho, Appl. Phys. Lett. **104**, 083512 (2014).

[35] A.M. Nardes, M. Kemerink, M.M. de Kok, E. Vinken, K. Maturova, and R.A.J. Janssen, Org. Electron. **9**, 727 (2008).

[36] T. Ohta, A. Bostwick, T. Seyller, K. Horn, and E. Rotenberg, Science **313**, 951 (2006).

[37] E. V. Castro, K.S. Novoselov, S. V. Morozov, N.M.R. Peres, J.M.B.L. Dos Santos, J. Nilsson, F. Guinea, A.K. Geim, and A.H.C. Neto, Phys. Rev. Lett. **99**, 216802 (2007).

[38] H.D. Lee, B. Magyari-Köpe, and Y. Nishi, Phys. Rev. B **81**, 193202 (2010).

[39] P.H. Holloway, J. Vac. Sci. Technol. **18**, 653 (1980).